THE ASTROPHYSICAL JOURNAL, 437:419–435, 1994 December 10

SiO MASER SURVEY OF THE GALACTIC BULGE *IRAS* SOURCES. I. THE $7° < |B| < 8°$ STRIPS

H. IZUMIURA,[1,2] S. DEGUCHI,[3] O. HASHIMOTO,[4] Y. NAKADA,[5] T. ONAKA,[6] T. ONO,[1,7]
N. UKITA,[3] AND I. YAMAMURA[6]

Received 1994 January 31; accepted 1994 June 17

ABSTRACT

We have surveyed Galactic bulge *IRAS* sources in the strips between $-15° < l < 15°$ and $7° < |b| < 8°$ in the SiO $J = 1$–0 $v = 1$ and 2 transitions. The sources were selected from the *IRAS* Point Source Catalogue based on the *IRAS* 12 and 25 μm flux densities, extracting dust-enshrouded objects at a distance of 8 kpc. SiO masers were detected in 53 of the 91 sources surveyed in these strips. Because distances to the *IRAS* sources in these strips have been known from the period-luminosity relation and periods of intensity variation at infrared wavelengths measured by others, the contamination by foreground sources in the sample can be checked relatively easily and the uncertainty in deriving physical parameters of the bulge is minimized. The detection rate of SiO masers does not depend much on the infrared colors in the selected color range (logarithm of the *IRAS* 25 to 12 μm flux density ratio between -0.15 and 0.3) and the detection rate increases with the 12 μm flux density of the *IRAS* sources. It has been found that the intrinsic SiO maser intensity depends weakly on the mass-loss rate for the bulge and disk SiO maser sources. No systematic difference of the SiO maser properties is found between bulge and disk sources. The radial velocities in the northern strip are shifted systematically from those in the southern strip by about 50 km s^{-1}. If this velocity shift is interpreted as due to a tilt of the bulge rotation axis to the galactic longitude circle, the tilt angle of the rotation of the bulge would be $18°(^{+18°}_{-14°})$. The angular rotation velocity of the bulge stellar system is 7.3×10^8 rad yr^{-1} (implying the rotation period of 8.6×10^7 yr). A Galactic top view of the distribution and the velocity vectors of the bulge SiO masers is given.

Subject headings: circumstellar matter — infrared: stars — masers — radio lines: stars — surveys — techniques: radial velocities

1. INTRODUCTION

The Galactic bulge is a stellar system of about 10^9 $M_\odot$ spread over about 2 kpc around the center of the Galaxy. Bulge stars belong to the old population (Frogel 1988) and may reveal the early history of the galactic evolution (Gilmore 1989). Due to dust extinction near the Galactic plane, optical observations of bulge stars are quite limited and possible only in a few optical windows (Frogel 1988). The overall structure of the bulge was revealed at infrared wavelengths by the *Infrared Astronomical Satellite* (*IRAS*). Habing et al. (1985) showed that the 25/12 μm flux density ratio from the *IRAS* Point Source Catalogue can be used to select bulge objects. *IRAS* sources with $\log (F_{25}/F_{12}) > -0.5$ are more likely to be associated with the Galactic bulge than the Galactic disk (Habing 1987). Rowan-Robinson & Chester (1987) have constructed a quantitative model for the infrared emission from bulge objects. A dynamical model of the bulge (Kent et al. 1992) was derived, based on the observed brightness distribution at 2.4 μm (Kent, Dame, & Fazio 1991).

From an analysis of the H I rotation curve, it has been considered that the bulge is not an axially symmetric spheroid but a triaxial or barlike structure (Manabe & Miyamoto 1975; Blitz & Spergel 1991a). Direct evidence for the bar structure of the bulge has recently been found by Blitz & Spergel (1991b) and Nakada et al. (1991) and a disk-bar feature similar to the bulge bar has been found by Weinberg (1992). Moreover, the Galactic bulge seems to be tilted with respect to the longitude circle ($l = 0°$) (Blitz & Spergel 1991b). It is interesting to look for the kinematic signature of the bar and the tilt of the bulge in the radial velocity sample of SiO maser sources.

Nakada et al. (1993) showed that color-selected samples of *IRAS* sources in the bulge very often exhibit SiO and H_2O maser emission at 43 and 22 GHz, respectively. The unexpected high detection rate (of about 65%) of SiO masers in Nakada et al.'s observations led us to plan a further rigorous survey of the bulge objects by observing SiO masers at 43 GHz with the Nobeyama 45 m telescope. We have surveyed about 300 color-selected *IRAS* sources in the SiO $J = 1$–0 $v = 1$ and $v = 2$ transitions at 43 GHz for the last 2 yr and have detected SiO masers in about 190 sources. Part of the preliminary results are reported elsewhere (Izumiura et al. 1993).

In this paper, we present the results of a part of this survey, i.e., the sources in the strips between $-15° < l < 15°$ and $7° < |b| < 8°$. The reason to restrict ourselves to sources in these strips in this paper is that many of them have known distances. Their near-infrared properties have been well studied by Whitelock, Feast, & Catchpole (1991). The periods of variation of infrared intensities for these sources have been measured and the distances to the sources are known from the period-luminosity relation. One of the difficulties of the bulge SiO maser survey is to distinguish the bulge and disk sources.

[1] Department of Astronomy and Earth Sciences, Tokyo Gakugei University, 4-1-1 Nukui-kita, Koganei, Tokyo 184, Japan.
[2] Current address: SRON Laboratory for Space Research Groningen, P.O. Box 800, NL-9700 AV Groningen, The Netherlands.
[3] Nobeyama Radio Observatory, National Astronomical Observatory, Minamimaki, Minamisaku, Nagano 384-13, Japan.
[4] Department of Applied Physics, Seikei University, 3-3-1 Kichijouji-kata, Musashino, Tokyo 180, Japan.
[5] Kiso Observatory, Institute of Astronomy, School of Science, The University of Tokyo, Mitake, Kiso, Nagano 397-01, Japan.
[6] Department of Astronomy, School of Science, The University of Tokyo, Bunkyo, Tokyo 113, Japan.
[7] Current address: Nishiharima Astronomical Observatory, Sayo-cho, Hyogo 679-53, Japan.

TABLE 1

OBSERVATION PERIODS

1.....	1991 Mar 10–17
2.....	1991 Apr 1–3
3.....	1991 Apr 22–23
4.....	1991 Apr 27–May 2
5.....	1991 Nov 18–25
6.....	1992 Jan 26–Feb 2
7.....	1992 May 11–16
8.....	1992 Jun 22–27
9.....	1992 Nov 24–29
10.....	1993 Apr 8–12
11.....	1993 Apr 26–May 3
12.....	1993 May 13–23

However, based on the derived distances, we can solve this problem at least for the sources in strips of $7° < |b| < 8°$, which are the subject of this paper.

2. OBSERVATIONS

Observations of the SiO $J = 1–0$ $v = 1$ and $v = 2$ masers at 43.122 and 42.821 GHz, respectively, were made during 1991 March–1993 May with the 45 m telescope at Nobeyama Radio Observatory[8] for the long-term key projects at Nobeyama Radio Observatory. The observing log is summarized in Table 1. We used a cooled SIS receiver (S40) for the 42 and 43 GHz observations and an acousto-optical spectrometer (AOS) having eight arrays with a 40 kHz resolution. The bandwidth of the receiver was about 0.4 GHz giving an effective radial velocity range of approximately ± 350 km s^{-1} in each line of SiO. The effective range of the velocity coverage varied slightly during each observation period due to tuning conditions at the band edges of the SIS receiver for the simultaneous observations of two separate lines of SiO. The overall system temperature was 180–600 K depending on the telescope elevation and weather conditions. The sensitivity of the SIS receiver at 43 GHz was improved by a factor of about 2 at the end of 1991, increasing the detection rate with respect to that of the observations in 1990 by Nakada et al. (1993). The half-power beamwidth of the telescope is 41″ and the aperture efficiency is 0.49 at 43 GHz. The antenna temperature used in this paper was corrected for ohmic loss and atmospheric attenuation but not for the beam or aperture efficiencies of the telescope. The conversion factor of the antenna temperature to the flux density is 3.6 Jy K^{-1}. All observations were made in the position switching mode using a 5′ off position in the azimuth direction. The pointing was checked every 2 hr with nearby SiO maser sources, W Hya, VX Sgr, and AH Sco, and the average pointing error was about 5″. The observed positions of the sources are from the *IRAS* Point Source Catalogue.

The source selection criteria were described in detail in Nakada et al. (1993). In addition, most of the sources are among the bulge *IRAS* sources selected by Whitelock et al. (1991) for the $|b| = 7°–8°$ strips. We summarize these selection criteria used in this paper below:

1. $|l| < 15°$.
2. $7° < |b| < 8°$.
3. $\delta > -40°$.
4. $-0.15 < \log(F_{25}/F_{12}) < 0.3$.
5. $F_{12} < 14$ Jy.

[8] Nobeyama Radio Observatory is a branch of the National Astronomical Observatory, an inter-university institute operated by the Ministry of Education, Science and Culture, Japan.

Here, F_{12} and F_{25} are flux densities at 12 and 25 μm in the *IRAS* Point Source Catalogue, respectively. In our experience (Nakada et al. 1993), these criteria are sufficient for the selection of bulge infrared sources with SiO masers. A simple estimate indicates that a dust enshrouded object of $T_{\rm eff} = 300$ K with 3000 $L_\odot$ at the distance of 8 kpc should have a flux density of 4.4 Jy at 12 μm, so that the above-mentioned criteria effectively select mass-losing stars with SiO masers in the Galactic bulge. We also observed several bright *IRAS* sources ($F_{12} > 14$ Jy) in this region and included these results here for the sake of completeness.

In this paper, we present observations of 91 sources in the strips between $7° < |b| < 8°$ only. The distribution of the observed sources in Galactic coordinates is shown in Figure 1. The observational results are shown in Table 2. Since the SiO maser intensity is strongly time variable, the observations were repeated several times (up to 4 times) for some sources, and the dates of observations are shown in Table 2 as date 1 and date 2. The date is expressed as 910315.1 etc., where the number shows the last two digits of the year (without 1900), month, day, and the observation time in the day (hour/24). We have detected the SiO lines in 53 of 91 observed sources. The lines were fitted by a Gaussian profile. The resulting peak intensity (T_a^*), peak radial velocity ($V_{\rm lsr}$), full width at half maximum (FWHM), and rms noise level (rms) for the spectra are summarized in Table 2 for the $v = 1$ and $v = 2$ transitions. The detection of the line was judged by identifying the signals in both spectra ($v = 1$ and 2). When the signal is weak, the "one line" identification becomes less convincing. However, our method of taking data for the $v = 1$ and 2 lines simultaneously secures the detection. We usually detected the $v = 1$ and $v = 2$ lines at almost the same radial velocity (within ± 1 km s^{-1}) except in IRAS 17599−3746 and IRAS 18282−2536, where they have a separation of about 3.7 and 1.0 km s^{-1}, respectively. The spectra of the SiO $J = 1–0$ $v = 1$ and 2 for the 53 sources detected are shown in Figures 2*a*–2*s*. The Gaussian line fitting is applied for all the sources with detected signals. However, the emission spectrum observed is not necessarily a Gaussian with a singly peaked profile. The fitting was made to

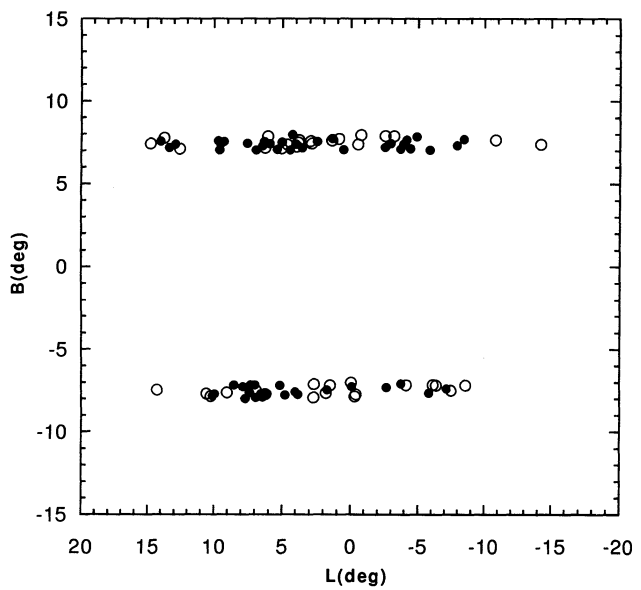

FIG. 1.—Distribution of the observed stars (*l*-*b* map). The filled circles indicate the stars with SiO maser, and the open circles without SiO maser.

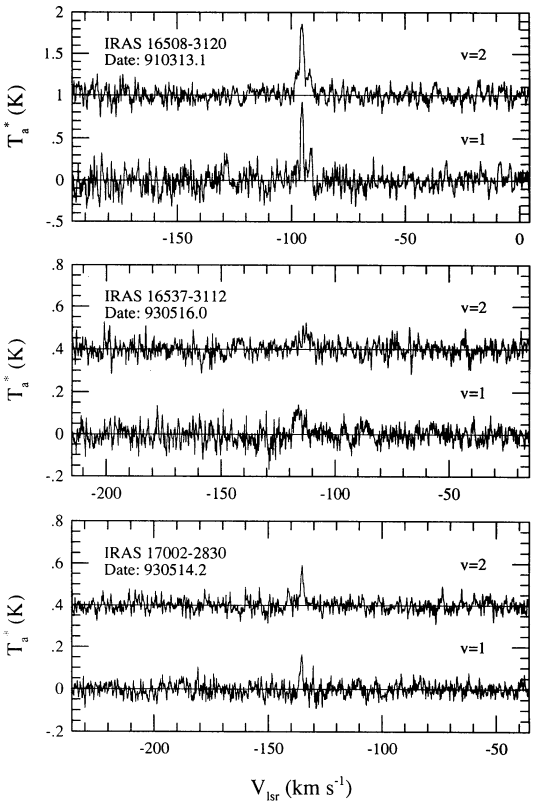

FIG. 2*a*

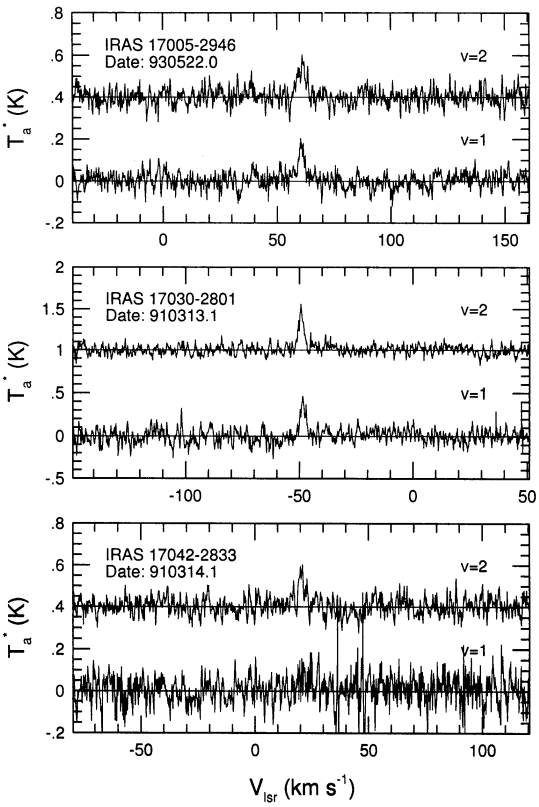

FIG. 2*b*

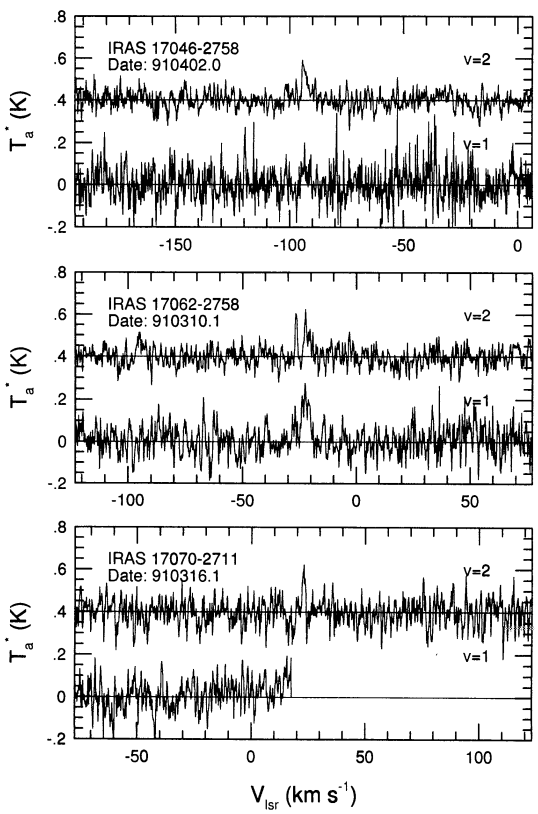

FIG. 2*c*

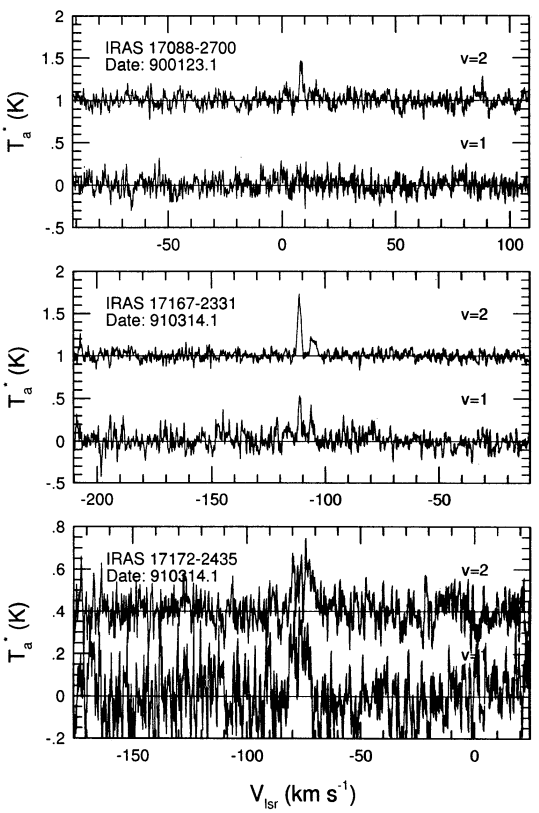

FIG. 2*d*

FIG. 2.—Spectra of the SiO $J = 1$–0 $v = 1$ and 2 for the 53 sources detected. The $J = 1$–0, $v = 1$ and 2 transitions are shown in Figs. 2*a*–2*r*. The time variation for IRAS 17440−1404 is shown in Fig. 2*s*.

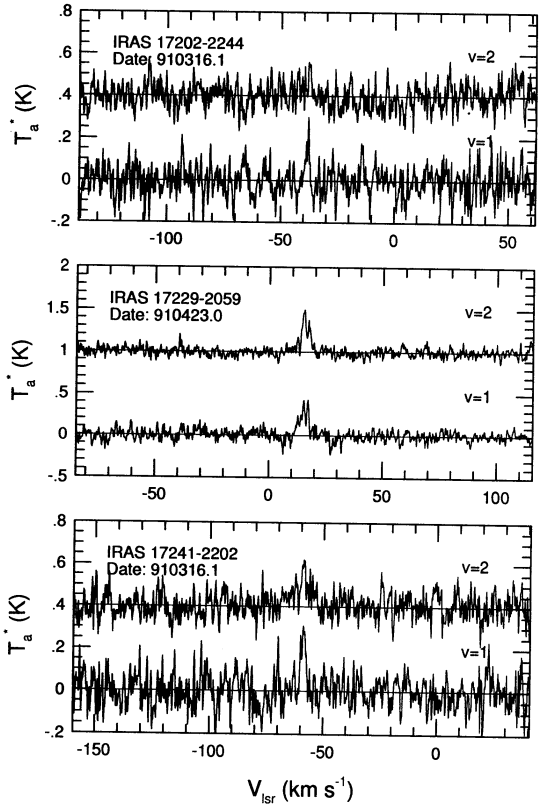

FIG. 2*e*

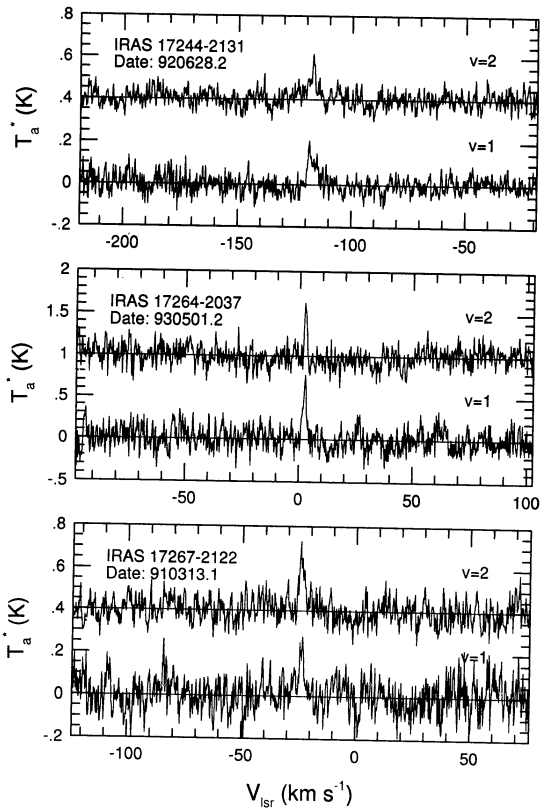

FIG. 2*f*

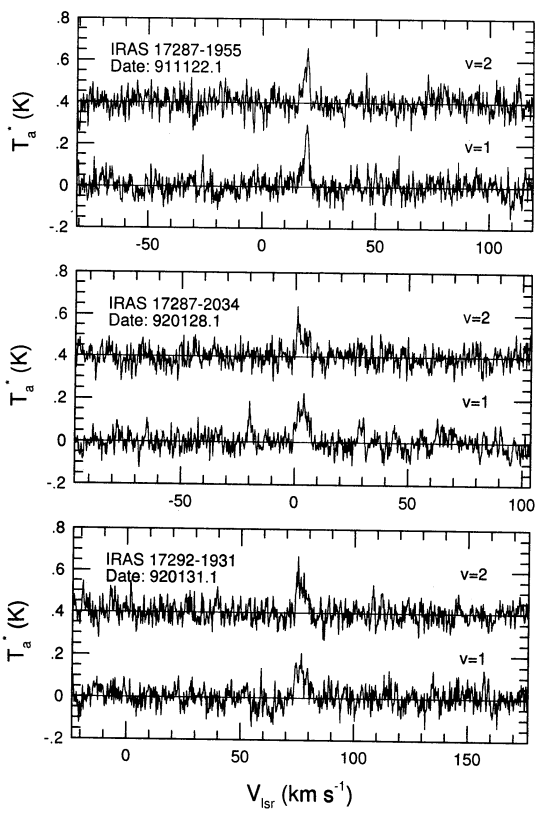

FIG. 2*g*

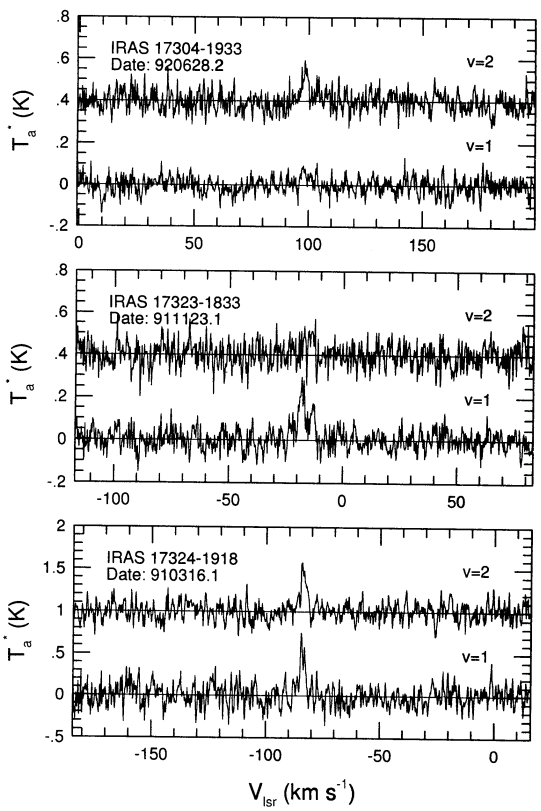

FIG. 2*h*

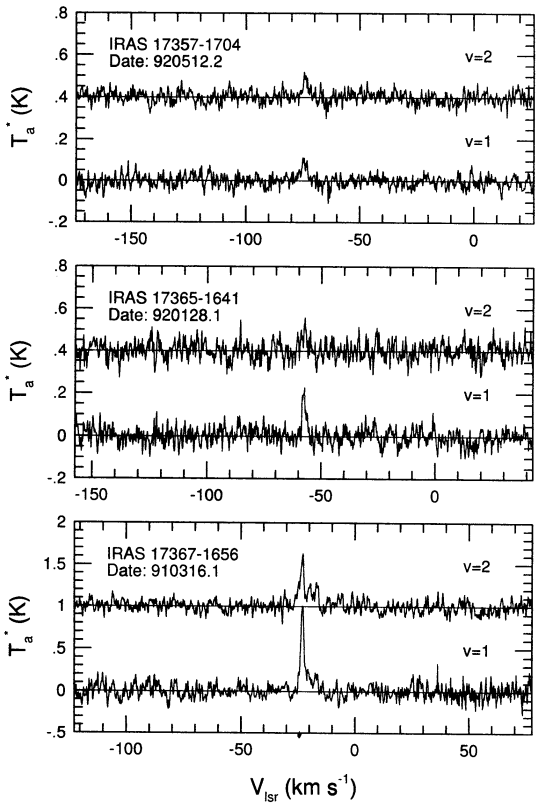

FIG. 2*i*

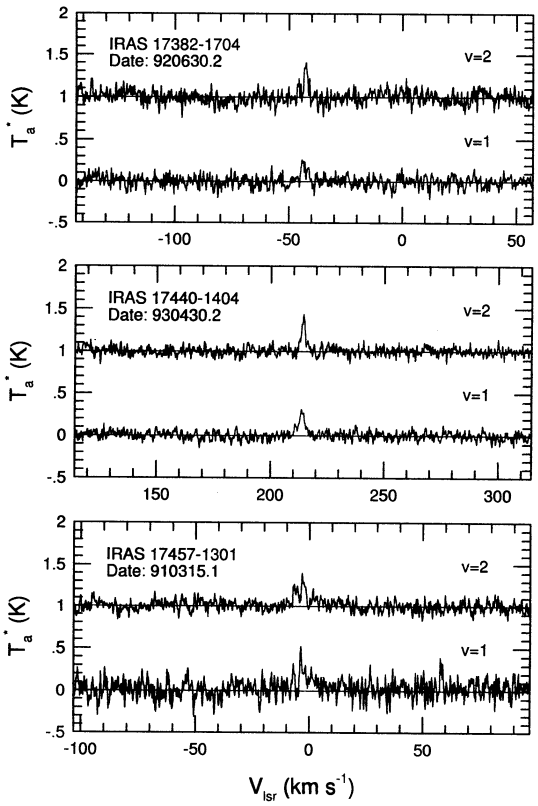

FIG. 2*j*

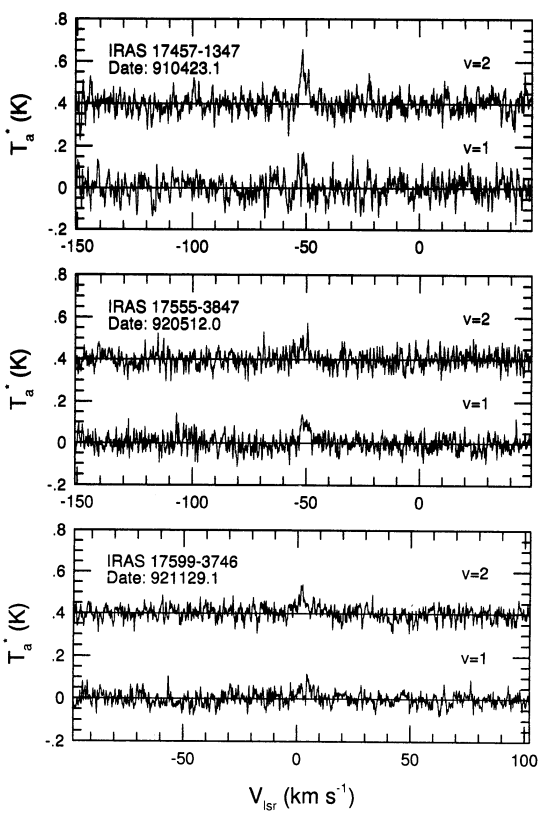

FIG. 2*k*

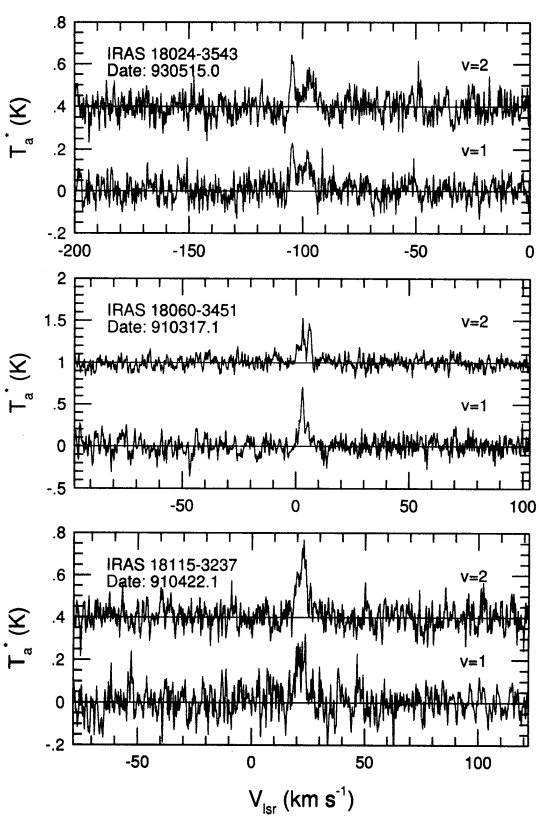

FIG. 2*l*

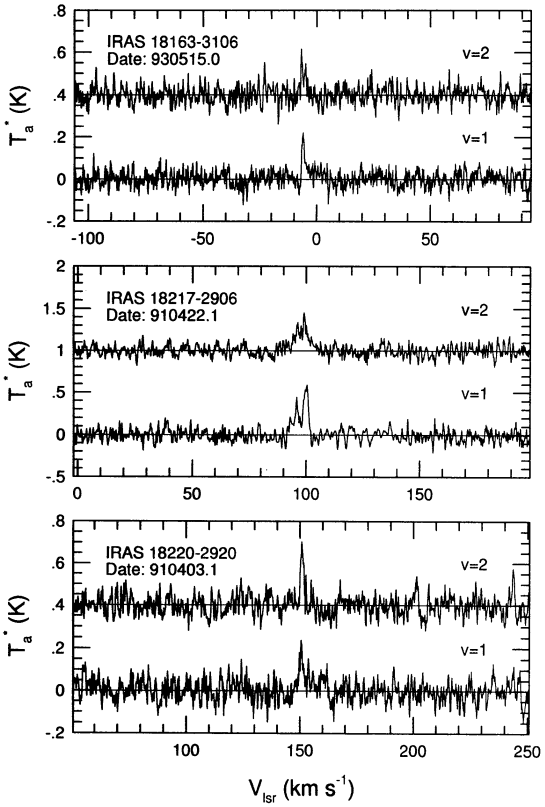

FIG. 2*m*

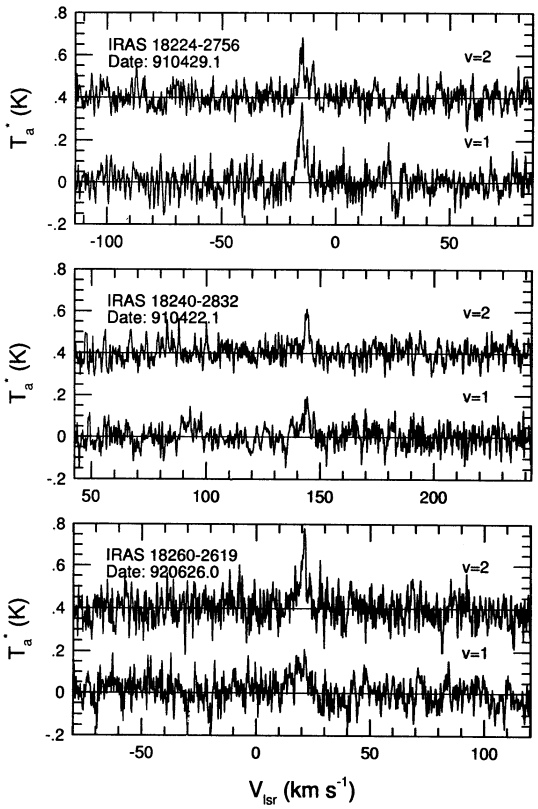

FIG. 2*n*

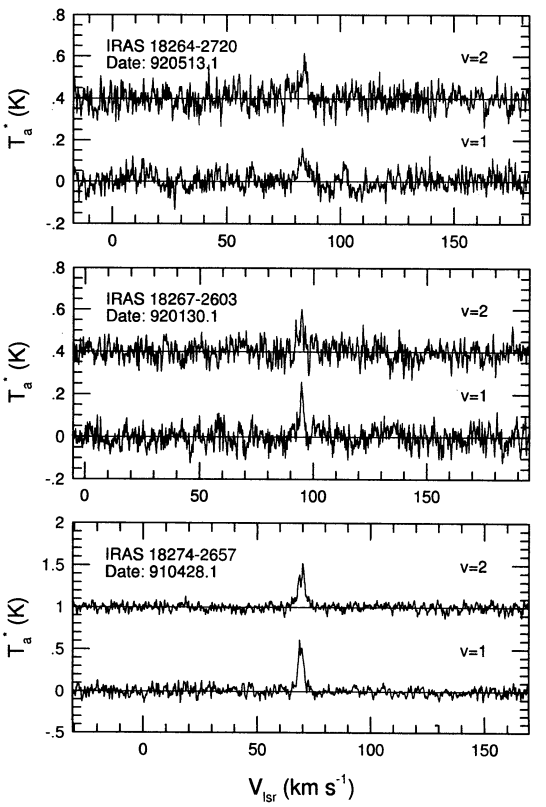

FIG. 2*o*

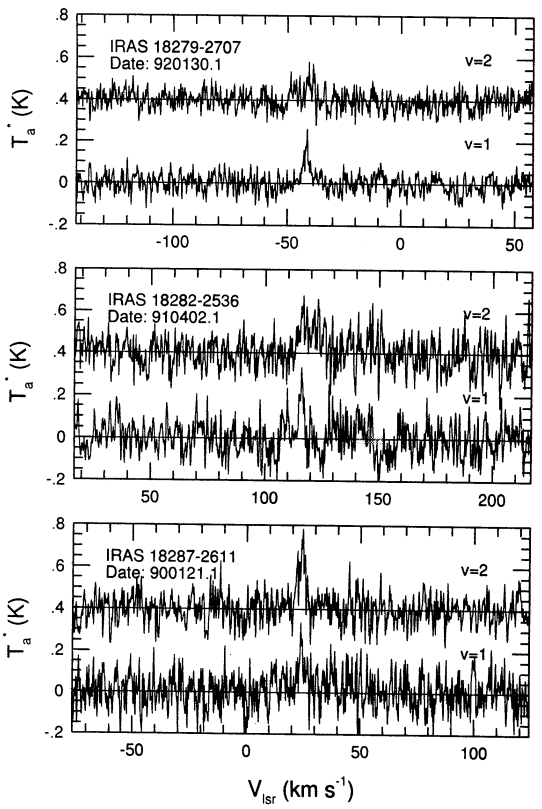

FIG. 2*p*

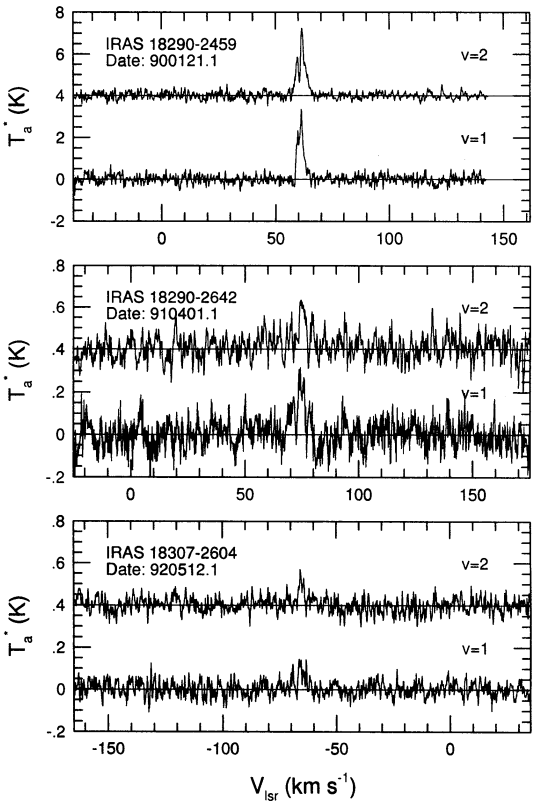

FIG. 2*q*

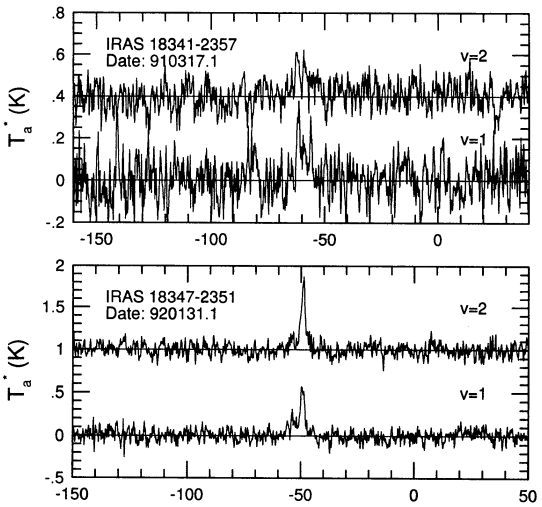

FIG. 2*r*

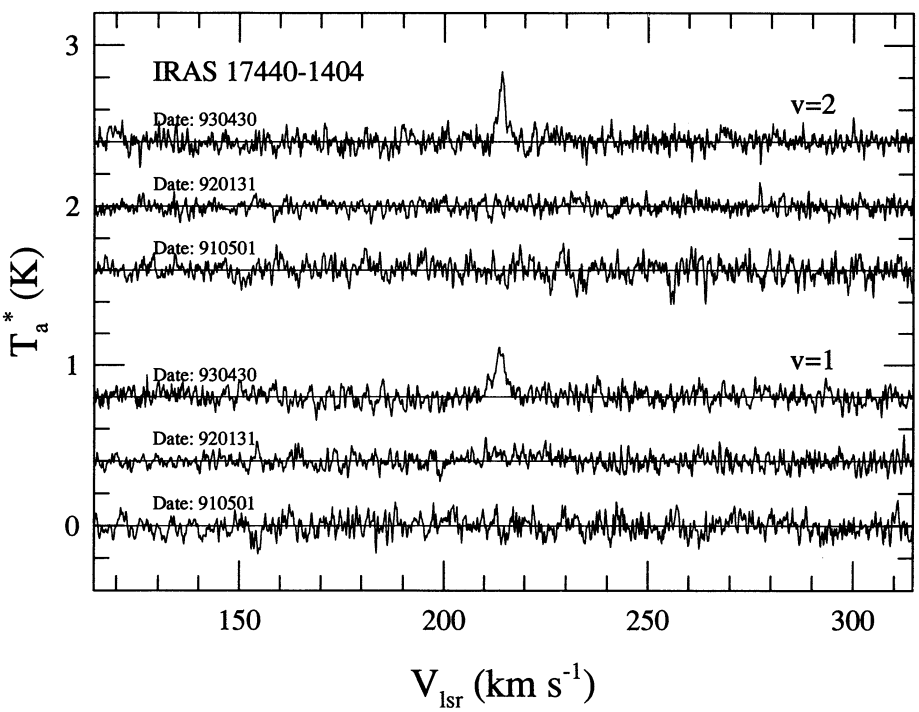

FIG. 2*s*

TABLE 2

LIST OF OBSERVED SOURCES

IRAS NUMBER	SiO $V=1, J=1$–0 T_a (K)	SiO $V=1, J=1$–0 V_{lsr} (km s^{-1})	SiO $V=1, J=1$–0 FWHM (km s^{-1})	SiO $V=1, J=1$–0 rms (K)	SiO $V=2, J=1$–0 T_a (K)	SiO $V=2, J=1$–0 V_{lsr} (km s^{-1})	SiO $V=2, J=1$–0 FWHM (km s^{-1})	SiO $V=2, J=1$–0 rms (K)	DATE 1 (yymmdd.h)	DATE 2 (yymmdd.h)
16342−3555	...	...	...	0.12	...	...	...	0.06	910315.0	921125.1
16439−3312	...	...	...	0.04	...	...	...	0.04	920128.0	930515.2
16508−3120	0.90	−95.59	1.32	0.13	0.67	−95.71	3.49	0.08	910313.0	
16537−3112	0.08	−114.92	5.52	0.04	0.05	−114.89	11.38	0.03	930516.0	
17002−2830	0.14	−135.50	1.40	0.03	0.12	−135.61	2.63	0.03	920128.0	930514.2
17005−2946	0.14	60.24	4.30	0.04	0.14	60.65	4.69	0.04	930522.0	
17030−2801	0.36	−49.01	3.05	0.10	0.45	−49.08	2.83	0.06	900122.0	910313.0
17042−2833	...	...	...	0.07	0.16	20.54	2.91	0.04	910314.0	
17046−2758	0.10	−93.51	2.64	0.08	0.16	−93.61	2.53	0.04	910402.0	
17047−2707	...	...	...	0.01	...	...	...	0.01	930515.0	
17062−2758	0.19	−22.87	4.83	0.07	0.08	−22.89	8.71	0.04	910310.0	
17064−2636	...	...	...	0.03	...	...	...	0.03	920512.0	
17070−2711	...	...	...	0.09	0.20	22.99	1.34	0.06	910316.0	
17088−2700	...	...	...	0.10	0.40	8.47	1.84	0.08	900123.0	
17107−2507	...	...	...	0.05	[0.16	−54.26	5.61	0.05	920131.0	
17134−2516	[0.09	−164.84	3.54]	0.02	...	...	...	0.03	930517.0	
17157−2355	...	...	...	0.02	...	...	...	0.02	930518.2	
17167−2331	0.26	−110.19	4.57	0.11	0.31	−110.27	4.36	0.06	910314.0	
17172−2435	0.27	−75.71	6.95	0.15	0.18	−75.68	9.95	0.08	910314.0	
17173−2334	...	...	...	0.03	...	...	...	0.03	930514.2	921128.1
17202−2244	0.23	−38.17	1.43	0.09	0.09	−38.16	2.87	0.06	910316.0	
17213−2219	...	...	...	0.11	...	...	...	0.06	910315.1	
17215−2228	...	...	...	0.03	...	...	...	0.03	920513.0	921126.1
17229−2059	0.30	15.11	5.13	0.06	0.35	15.71	4.86	0.05	910423.0	
17230−2135	...	...	...	0.02	...	...	...	0.02	930516.2	
17237−2138	...	...	...	0.04	...	...	...	0.04	920513.0	930427.2
17241−2202	0.24	−59.44	2.86	0.08	0.12	−59.44	10.16	0.06	910316.0	
17244−2131	0.12	−118.81	4.59	0.04	0.09	−118.81	7.31	0.04	910401.0	920628.2
17249−2140	...	...	...	0.02	...	...	...	0.00	920131.0	921127.0
17260−2101	...	...	...	0.02	...	...	...	0.02	920628.2	930513.2
17264−2037	0.66	2.57	1.87	0.14	0.63	2.59	1.17	0.12	920514.2	930501.2
17267−2122	0.21	−23.98	2.86	0.09	0.26	−24.01	2.72	0.06	910313.0	
17275−1933	...	...	...	0.01	...	...	...	0.01	930519.2	
17278−2048	...	...	...	0.03	...	...	...	0.03	930410.0	
17287−1955	0.21	19.26	3.81	0.05	0.17	19.07	3.53	0.05	900123.0	911122.1
17287−2034	0.17	3.68	5.39	0.04	0.10	3.71	6.41	0.04	920128.0	
17292−1931	0.14	76.09	5.55	0.04	0.15	76.40	4.67	0.05	910316.0	920131.0
17304−1933	0.05	99.16	6.03	0.05	0.11	99.12	4.74	0.05	910403.0	920628.2
17304−1947	...	...	...	0.04	...	...	...	0.04	910313.0	920131.0
17323−1833	0.17	−16.89	7.39	0.05	0.06	−16.87	7.42	0.06	911123.1	
17324−1918	0.57	−84.05	2.79	0.14	0.46	−84.08	3.36	0.10	910316.0	
17357−1704	0.08	−73.90	3.54	0.03	0.09	−73.86	2.88	0.03	910428.0	920512.2
17365−1641	0.19	−57.36	2.07	0.04	0.09	−57.34	3.41	0.04	911123.1	920128.0
17367−1656	0.71	−22.46	3.04	0.09	0.35	−22.47	5.38	0.07	910316.0	
17382−1704	0.19	−42.90	3.60	0.06	0.37	−42.92	1.85	0.07	910310.0	920630.2
17440−1404	0.26	213.66	3.84	0.05	0.26	214.49	4.07	0.05	920131.0	930430.2
17443−1431	...	...	...	0.03	...	...	...	0.03	921124.1	930430.2
17445−1308	...	...	...	0.05	...	...	...	0.05	910310.1	
17457−1301	0.31	−3.13	3.38	0.14	0.23	−3.15	5.53	0.06	910315.0	
17457−1347	0.15	−50.82	1.84	0.05	0.16	−50.76	3.97	0.05	910423.0	
17478−1227	...	...	...	0.02	...	...	...	0.02	920510.2	930515.2
17509−3956	...	...	...	0.04	...	...	...	0.04	930517.1	
17552−3909	...	...	...	0.07	...	...	...	0.04	910427.0	921128.0
17555−3847	0.11	−51.10	3.96	0.04	0.07	−51.04	5.80	0.04	910502.0	920512.0
17566−3801	...	...	...	0.04	...	...	...	0.05	930429.0	911118.1
17570−3748	...	...	...	0.04	...	...	...	0.04	930515.0	
17599−3746	0.06	5.94	7.65	0.03	0.10	2.24	2.99	0.03	910429.0	921129.1
18018−3605	...	...	...	0.05	...	...	...	0.06	910423.0	911124.0
18024−3542	0.13	−99.90	10.06	0.04	0.10	−99.91	11.35	0.05	930515.0	
18060−3451	0.51	2.99	3.14	0.10	0.28	3.01	6.48	0.07	910317.0	
18106−3226	...	...	...	0.05	...	...	...	0.04	910423.0	
18115−3237	0.21	21.63	5.71	0.06	0.27	22.03	5.25	0.05	910422.0	
18129−3305	...	...	...	0.03	...	...	...	0.04	920130.0	930521.0
18136−3303	...	...	...	0.02	...	...	...	0.03	930515.0	
18146−3110	...	...	...	0.02	...	...	...	0.03	930409.0	
18163−3106	0.21	−6.05	1.35	0.04	0.12	−6.09	2.89	0.04	920512.0	930515.0
18169−3006	...	...	...	0.05	...	...	...	0.06	910427.0	920629.0
18173−3107	...	...	...	0.04	...	...	...	0.04	910317.0	920629.0

TABLE 2—*Continued*

IRAS Number	SiO $V = 1, J = 1$–0 T_a (K)	V_{lsr} (km s^{-1})	FWHM (km s^{-1})	rms (K)	SiO $V = 2, J = 1$–0 T_a (K)	V_{lsr} (km s^{-1})	FWHM (km s^{-1})	rms (K)	Date 1 (yymmdd.h)	Date 2 (yymmdd.h)
18204−3027.....	...	...	...	0.04	...	...	...	0.03	910402.0	921128.1
18217−2906.....	0.36	98.36	6.38	0.07	0.28	98.24	7.03	0.06	910422.0	
18220−2920.....	0.13	151.34	4.18	0.06	0.24	150.73	2.10	0.04	910403.0	
18224−2756.....	0.20	−13.83	5.76	0.05	0.14	−13.79	6.54	0.05	910429.0	
18240−2832.....	0.10	143.06	6.56	0.05	0.09	142.60	6.51	0.02	910422.0	
18260−2619.....	0.12	19.26	8.76	0.07	0.19	20.26	6.18	0.07	910429.0	920626.0
18264−2720.....	0.11	83.75	4.85	0.04	0.12	83.08	4.39	0.05	911123.1	920513.0
18267−2603.....	0.14	94.01	3.48	0.04	0.13	94.88	3.00	0.04	910317.0	920130.1
18267−2715.....	...	...	...	0.04	...	...	...	0.04	910429.0	920626.0
18273−2632.....	...	...	...	0.04	...	...	...	0.04	910418.0	
18274−2657.....	0.54	69.34	2.88	0.05	0.41	69.40	3.68	0.04	910428.0	
18279−2707.....	0.16	−42.06	3.50	0.04	0.06	−42.08	9.66	0.04	920130.1	
18282−2536.....	0.26	115.81	2.22	0.08	0.17	116.82	4.25	0.06	910402.0	
18287−2611.....	0.20	24.42	3.58	0.08	0.26	24.04	4.31	0.06	900121.1	
18290−2459.....	2.42	61.41	3.42	0.21	2.22	61.56	4.39	0.17	900121.1	
18290−2642.....	0.27	74.73	2.96	0.08	0.23	75.04	2.87	0.05	910401.0	
18307−2604.....	0.08	−64.86	5.00	0.03	0.10	−64.90	3.68	0.04	920512.0	
18319−2442.....	...	...	...	0.03	...	...	...	0.03	930519.0	
18341−2357.....	0.20	−60.14	5.28	0.11	0.13	−60.14	7.49	0.07	910317.0	
18347−2351.....	0.44	−49.85	3.57	0.07	0.53	−49.92	3.73	0.07	910317.0	920131.1
18351−2325.....	...	...	...	0.03	...	...	...	0.03	920131.1	930514.0
18351−2345.....	...	...	...	0.08	...	...	...	0.05	910313.0	
18414−1959.....	...	...	...	0.03	...	...	...	0.04	920130.1	

adjust the integrated intensity of the Gaussian profile being equal to the total area of emission. With this method, the uncertainty of V_{lrs} is estimated to be less than 1 km s^{-1}.

A strong signal appears, occasionally, only in the $v = 2$ transition, e.g., in IRAS 17042−2833 (Fig. 2*b*). We did not consider this type of a single signal as a SiO maser except when it is a very strong broad signal line in IRAS 17042−2833. Two sources (IRAS 17107−2507 and IRAS 17134−2516) show a weak (3 or 4 σ) emission feature only in one vibrational state and should be counted as probable detections and shown between the square brackets in Table 2. These data are not used in the later analysis.

The SiO maser intensity varies with time. For example, no signal was detected in IRAS 17440−1404 on 1991 May 1, and 1992 January 31, but strong emission was detected at V_{lsr} = 210 km s^{-1} on 1993 April 30 (Fig. 2*s*).

3. DISCUSSION

The infrared properties of the observed sources are listed in Table 3. The flux densities at 12, 25, and 60 μm are taken from the *IRAS* Point Source Catalogue and the colors are calculated from the flux densities: $C[25/12] = \log (F25/F12)$ and $C[60/25] = \log (F60/F25)$. For 75 sources, the periods of the brightness variation in the infrared K-band were measured by Whitelock et al. (1991). In Table 3, the distance moduli $(m - M_0)$, and the logarithm of the mass-loss rate, $\log [\dot{M}(M_\odot\ \mathrm{yr}^{-1})]$, are also shown (taken from Whitelock et al. 1991). The distance moduli were derived from the period-luminosity relation adopting a distance to the Galactic center of 8.6 kpc. The mass loss rates were deduced by Whitelock et al. (1991) from the infrared luminosity (from observations at 12 μm and *K*-band together with the evaluated distances). Of 53 sources with detected SiO masers, 47 sources have known periods and 33 sources among them are the sources within a distance of 2.5 kpc from the Galactic center judging from the distance moduli. These 33 sources are probably real bulge sources (e.g., Deguchi, Nakada, & Sahai 1990; Cho, Kaifu, & will first discuss the global properties of detected SiO sources.

3.1. *The* SiO *Detection Rate*

The overall detection rate of the SiO masers for the sources in the 7°–8° strips is 58% ≈ 53/91 for the $v = 2$ transition and 56% ≈ 51/91 for $v = 1$. These detection rates are much higher than the detection rate of SiO masers for much closer *IRAS* sources (e.g., Deguchi, Nakada, & Sahai 1990; Cho, Kaifu, & Ukita 1993). Though the sensitivity of the telescope was improved by a factor of 2 meanwhile, the detection rate for the $v = 2$ transition is in fact slightly lower than 65%, the rate previously obtained by Nakada et al. (1993), since we tried much fainter *IRAS* sources in this survey.

Figure 3*a* shows a histogram of the 12 μm flux density of the detected and undetected sources. The detection rate decreases with decreasing the 12 μm flux density, since the distance increases with decreasing infrared intensity. Figure 3*b* shows a histogram of the infrared color, $C[25/12][=\log (F_{25}/F_{12})]$ of the detected and undetected sources. The detection rate does not vary significantly with color within the color selection range in this sample. The decrease of the detection rate with decreasing *IRAS* 12 μm flux and the relatively flat detection rate with infrared color imply that we are studying a rather homogeneous source sample in this survey.

3.2. *Discrimination of the Disk Sources from the Sample*

Whitelock et al. (1986, 1991) have obtained an extensive near-infrared JHKL photometry of *IRAS* objects in the direction of the Galactic bulge. In particular, the sources in the two strips between $7° < |b| < 8°$ across the bulge have been monitored for 4–5 yr and the periods of infrared time variations were obtained. The distance moduli were derived from the period-luminosity relation for Large Magellanic Cloud Mira variables and Galactic globular clusters, etc. (for example, Feast 1987). Following Whitelock et al. (1991), we assume a

TABLE 3

INFRARED PROPERTIES OF THE OBSERVED SOURCES

IRAS Name	l	b	F_{12} (Jy)	$C[25/12]$[a]	$C[60/25]$[b]	P (day)	$(m - M_0)$ (mag)	log $(\dot{M})$[c]
16342−3555.....	−14°20	7°39	1.72	0.02	−0.09			
16439−3312.....	−10.81	7.67	2.66	−0.13	−0.63	403	15.1	−5.44
16508−3120.....	−8.42	7.72	13.40	−0.08	−0.65	677	14.1	−4.53
16537−3112.....	−7.92	7.33	1.25	−0.08	−0.32	455	14.9	−5.22
17002−2830.....	−4.89	7.86	1.93	0.04	−0.59	433	14.8	−5.22
17005−2946.....	−5.87	7.04	0.97	0.14	−0.45	486	15.4	−5.19
17030−2801.....	−4.14	7.67	9.65	0.13	−0.55	722	14.6	−4.57
17042−2833.....	−4.41	7.13	3.99	0.02	−0.61	715	15.5	−4.62
17046−2758.....	−3.88	7.41	1.98	−0.10	−0.26	490	15.3	−4.84
17047−2707.....	−3.18	7.89	1.40	−0.15	−0.32	445	15.2	−5.02
17062−2758.....	−3.67	7.12	11.93	−0.09	−0.90	511	13.3	−4.86
17064−2636.....	−2.53	7.89	1.63	0.04	−0.58	545	14.9	−5.29
17070−2711.....	−2.94	7.45	9.87	−0.01	−0.19			
17088−2700.....	−2.54	7.22	13.09	0.14	−0.49			
17107−2507.....	−0.74	7.97	2.19	0.23	−0.50			
17134−2516.....	−0.53	7.40	1.16	−0.05	−0.30	397	14.4	−5.43
17157−2355.....	0.89	7.74	1.13	−0.05	−0.38	257	14.9	−5.34
17167−2331.....	1.36	7.76	7.81	−0.10	−0.68			
17172−2435.....	0.54	7.07	5.37	−0.11	−0.73	441	13.7	−5.72
17173−2334.....	1.40	7.62	1.68	0.25	−0.48			
17202−2244.....	2.47	7.55	5.74	−0.13	−0.71	429	13.3	−5.89
17213−2219.....	2.97	7.58	38.45	−0.15	−0.74			
17215−2228.....	2.88	7.44	10.64	0.10	−0.77			
17229−2059.....	4.30	7.99	3.42	0.00	−0.73	517	14.8	−4.97
17230−2135.....	3.81	7.65	1.28	−0.12	−0.32	301	14.3	−6.09
17237−2138.....	3.85	7.49	4.29	−0.11	−0.45	237	13.8	−5.47
17241−2202.....	3.56	7.18	5.40	−0.04	−0.68	592	14.4	−4.87
17244−2131.....	4.04	7.42	2.45	0.14	−0.55	428	14.5	−5.16
17249−2140.....	3.98	7.24	2.13	−0.01	−0.67	480	14.8	−5.15
17260−2101.....	4.67	7.37	1.60	−0.03	−0.53	454	14.7	−5.30
17264−2037.....	5.06	7.52	3.39	0.03	−0.63	465	15.0	−4.91
17267−2122.....	4.46	7.04	4.08	0.18	−0.50	533	15.2	−4.57
17275−1933.....	6.11	7.87	1.08	−0.10	−0.31	409	15.5	−5.00
17278−2048.....	5.08	7.14	1.21	0.03	−0.40			
17287−1955.....	5.94	7.44	8.34	0.17	−0.62	578	14.5	−4.55
17287−2034.....	5.40	7.09	2.61	−0.07	−0.61			
17292−1931.....	6.36	7.56	6.52	−0.13	−0.72	556	14.6	−5.29
17304−1933.....	6.47	7.31	2.24	0.17	−0.56	537	15.7	−4.65
17304−1947.....	6.27	7.18	4.07	0.05	−0.76	538	15.1	−4.80
17323−1833.....	7.57	7.46	2.84	−0.12	−0.67	596	14.6	−5.63
17324−1918.....	6.94	7.04	4.08	0.11	−0.69			
17357−1704.....	9.27	7.55	3.87	0.07	−0.81	500	14.7	−5.01
17365−1641.....	9.71	7.60	2.06	−0.14	−0.44	408	15.0	−5.59
17367−1656.....	9.51	7.43	6.96	−0.02	−0.72	628	14.2	−4.85
17382−1704.....	9.59	7.05	22.79	−0.04	−0.67	477	12.8	−4.88
17440−1404.....	12.90	7.41	1.80	0.00	−0.57	435	14.4	−5.40
17443−1431.....	12.56	7.11	1.46	−0.09	−0.42			
17445−1308.....	13.77	7.79	10.67	−0.13	−0.92			
17457−1301.....	14.03	7.58	6.89	−0.10	−0.63	461	13.7	−4.92
17457−1347.....	13.36	7.20	3.93	−0.15	−0.71	434	14.2	−5.64
17478−1227.....	14.79	7.43	1.45	−0.13	−0.34	422	15.3	−5.65
17509−3956.....	−8.58	−7.17	1.22	−0.12	−0.28	526	14.9	−5.88
17552−3909.....	−7.47	−7.51	1.96	0.13	−0.44	498	15.7	−4.84
17555−3847.....	−7.12	−7.38	1.99	−0.12	−0.56	461	15.4	−5.48
17566−3801.....	−6.35	−7.19	3.06	−0.03	−0.63	646	15.2	−4.82
17570−3748.....	−6.12	−7.14	1.49	−0.15	0.23	366	14.9	−5.76
17599−3746.....	−5.80	−7.64	2.86	−0.05	−0.53	463	14.6	−5.04
18018−3605.....	−4.13	−7.16	3.72	0.01	−0.73	590	14.9	−4.91
18024−3543.....	−3.75	−7.07	1.70	−0.12	−0.40	474	16.0	−5.31
18060−3451.....	−2.63	−7.31	13.46	−0.13	−0.70	439	13.0	−5.61
18106−3226.....	−0.02	−7.00	3.20	−0.15	−0.69			
18115−3237.....	−0.09	−7.26	4.02	0.05	−0.39			
18129−3305.....	−0.38	−7.73	2.14	−0.11	−0.59	496	15.7	−5.31
18136−3303.....	−0.28	−7.86	1.37	−0.07	−0.37	389	15.3	−4.93
18146−3110.....	1.51	−7.17	1.49	0.18	−0.45	525	15.6	−4.82
18163−3106.....	1.74	−7.46	1.85	0.01	−0.64	419	14.2	−5.46
18169−3006.....	2.69	−7.11	2.65	0.02	−0.54	496	14.8	−5.22
18173−3107.....	1.81	−7.65	6.09	−0.06	−0.74	582	14.5	−4.76
18204−3027.....	2.72	−7.93	2.44	−0.01	−0.62	423	14.9	−5.07
18217−2906.....	4.07	−7.58	5.20	−0.11	−0.59	534	14.4	−5.46

TABLE 3—*Continued*

IRAS Name	l	b	F_{12} (Jy)	C[25/12][a]	C[60/25][b]	P (day)	$(m - M_0)$ (mag)	log ($\dot{M}$)[c]
18220−2920.....	3.88	−7.73	2.24	−0.15	−0.60	476	14.7	−5.66
18224−2756.....	5.18	−7.17	3.79	−0.13	−0.67	496	14.4	−5.57
18240−2832.....	4.81	−7.77	4.33	−0.13	−0.68	514	15.1	−5.26
18260−2619.....	7.01	−7.15	3.91	−0.02	−0.60	508	14.6	−4.91
18264−2720.....	6.13	−7.69	8.93	0.02	−0.68	660	14.6	−4.62
18267−2603.....	7.31	−7.16	6.63	−0.06	−0.71	552	14.7	−4.62
18267−2715.....	6.24	−7.71	3.45	0.01	−0.76	512	14.6	−5.04
18273−2632.....	6.94	−7.51	4.43	0.06	−0.68	224	13.5	−5.41
18274−2657.....	6.58	−7.72	3.63	−0.14	−0.65	471	14.5	−5.56
18279−2707.....	6.47	−7.89	2.21	0.13	−0.64	392	14.7	−5.20
18282−2536.....	7.87	−7.26	3.37	−0.06	−0.79	512	14.9	−4.85
18287−2611.....	7.40	−7.62	8.63	0.11	−0.66	666	14.6	−4.64
18290−2459.....	8.51	−7.15	31.62	0.00	−0.66	452	11.3	−5.41
18290−2642.....	6.97	−7.93	2.59	−0.03	−0.55	471	14.9	−5.02
18307−2604.....	7.71	−7.99	1.58	−0.14	−0.42	404	14.5	−5.93
18319−2442.....	9.06	−7.62	1.29	−0.05	−0.32	443	15.0	−5.21
18341−2357.....	9.96	−7.72	9.39	−0.13	−0.66	517	14.5	−5.15
18347−2351.....	10.12	−7.80	6.33	−0.07	−0.68	575	14.4	−4.77
18351−2325.....	10.56	−7.69	1.52	−0.13	−0.45	373	14.9	−5.78
18351−2345.....	10.24	−7.83	6.93	0.03	−0.94			
18414−1959.....	14.30	−7.45	1.40	−0.03	−0.46	441	14.7	−5.34

[a] $C[25/12] = \log(F_{25}/F_{12})$.
[b] $C[60/25] = \log(F_{60}/F_{25})$.
[c] log ($\dot{M}$) = logarithm of the mass-loss rate ($M_\odot$ yr^{-1}).

distance to the Galactic center of $R_0 = 8.6$ kpc (Feast 1987; Reid et al. 1988) and a distance modulus of the Galactic center of 14.7 mag. The detection rate of SiO masers as a function of distance modulus in Figure 4 decreases with distance modulus when it is larger than 15, indicating simply that distant SiO masers are difficult to detect.

Among the 75 sources for which periods are measured by Whitelock et al. (1991), SiO masers were detected in 47 sources. These sources are listed in Table 4, giving the radial velocity with respect to the Galactic standard of rest (corrected for the Galactic rotation, 220 km s^{-1}, of the LSR; see Kerr & Lynden-Bell 1986), $V_s = (V_{lsr} + 220 \sin l \cos b$ km s^{-1}), the circular rotation velocity around the galactic center, V_{rot} (calculated assuming V_s is the projected velocity of V_{rot} on the line of sight), integrated intensities of the SiO maser for the $v = 1$ and 2 transition (adapted the distance of 8.6 kpc for the normalization), I ($v = 1$ and 2), respectively, and the distance from the Galactic center, R (calculated from the distance modulus). It indicates that 33 sources are within 2.5 kpc from the Galactic center and the other 14 sources are beyond 2.5 kpc from the Galactic center. Hereafter, we will refer to the former as bulge sources and the latter as disk sources.

The discrimination of the disk sources from the present samples chiefly depends on the period-luminosity relation derived by Whitelock et al. (1991) which is derived from the observations of Mira stars in Large Magellanic Cloud (LMC) and OH/IR sources in our Galaxy. Judging from Figure 10 in Whitelock et al. (1991), the data points deviate from the best fit line approximately by about 0.2 mag for the LMC stars with period less than 500 days and by 1 mag for OH/IR sources with periods more than 500 days. This corresponds to the mean errors in the luminosity estimation of about 25% for

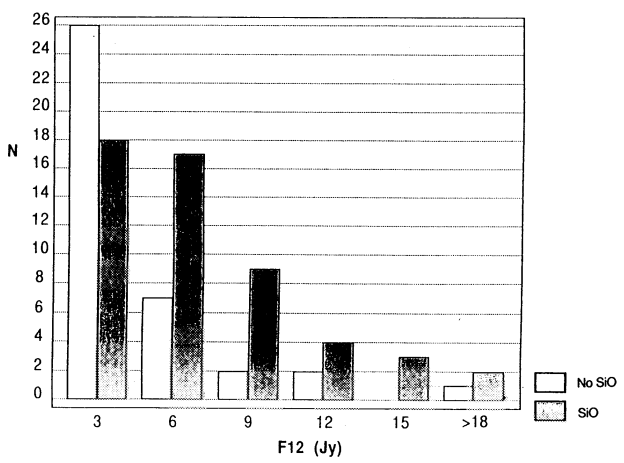

FIG. 3*a*

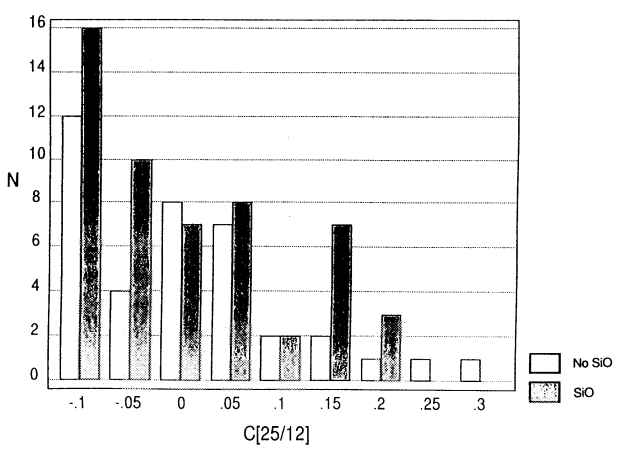

FIG. 3*b*

FIG. 3.—Histogram of (*a*) the *IRAS* 12 μm flux density, *F*12, (*b*) colors, log (*F*25/*F*12), for the detected and undetected sources. Gray rectangles indicate the detected sources, and white ones, the undetected.

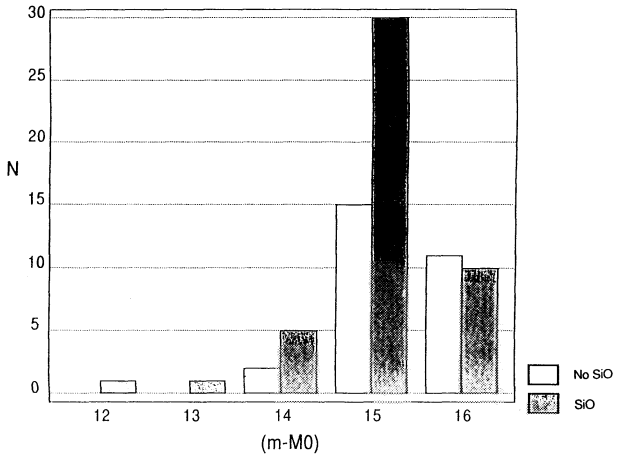

FIG. 4.—Histogram of the distance moduli for the detected and undetected sources. Gray rectangles indicate the detected sources, and white ones, the undetected. The detection rate drops at $(m - M_0) > 15$.

LMC Mira variables and 150% for the Galactic OH/IR stars, giving the errors in distance estimation by about 12% to 60%. The further investigation of the local Mira variables (Whitelock et al. 1994) demonstrated that local Mira variables are not necessarily fainter at K magnitude than those with the same period in LMC. Figure 14 of Whitelock et al. (1994) gives the errors in the estimation of the bolometric magnitude about 0.25 mag. From these facts, we believe that the errors in the distance estimation for the bulge sources from the period-luminosity relation are within about 20% (perhaps more for the longer period sources).

The bulge stars belong to the old population, and they are supposed to be metal poor (see Frogel 1988). It is possible that the properties of the bulge and disk SiO masers are different. Wood et al. (1992) found that OH/IR stars in the Large Magellanic Cloud (supposed to be Population II) have lower expansion velocities than the comparable OH/IR sources in our Galaxy. Though a number of SiO maser pumping mechanisms were studied so far (see Bujarrabal 1994), the effect of abundance variation of the SiO molecule in the circumstellar envelope on the intensity ratio of the $v = 1$ to $v = 2$, $J = 1$–0 line has not necessarily been clarified yet.

To see whether or not the properties of bulge and disk SiO maser sources are different, we have plotted the logarithm of integrated intensities for $v = 1$ and $v = 2$ in Figure 5. The filled circles and open triangles indicate bulge and disk sources, respectively. The integrated intensities show a large spread for the disk sources, but, the sources on average follow the relation, $I(v = 1) = I(v = 2)$. The bulge sources do not seem to deviate much from it. The slight difference in the y-intercept of the fitted line in Figure 5 probably comes from the difference in sensitivity between the $v = 1$ and $v = 2$ observations. The rms noise level in the $v = 1$ spectrum is higher by about 50% than that in the $v = 2$ spectrum, so the obtained integrated intensities for the $v = 1$ transitions deviate more from the averages than those in the $v = 2$ transitions do. We conclude that the intensity ratio of the $v = 1$ to $v = 2$ transition are not different between the bulge and disk sources.

We have also plotted in Figure 6 the integrated intensity of the SiO masers (in units of Jy km s^{-1} at a distance of 8.6 kpc) versus the logarithm of the mass-loss rate. The best fit lines are $I(v = 2) = 1.25[\dot{M}/1 \times 10^{-6}(M_\odot\ \mathrm{yr}^{-1})]^{0.251}$ Jy km s^{-1} for the

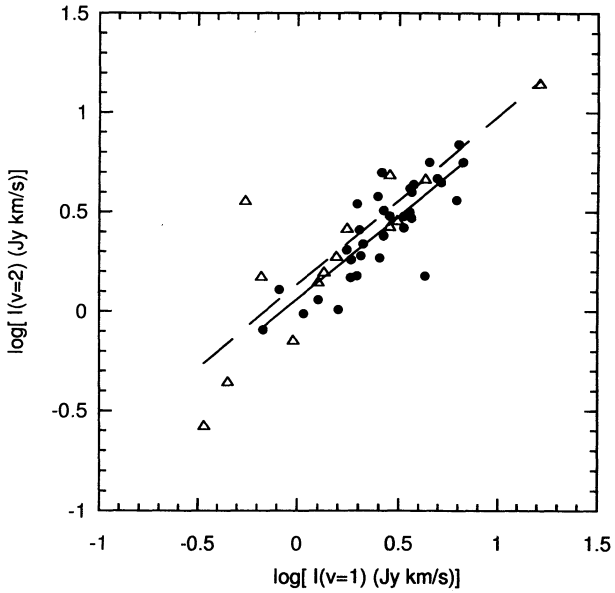

FIG. 5.—Comparison of the integrated intensity (corrected for the distance) between $v = 1$ and $v = 2$. Filled circles are bulge sources, and triangles are disk sources. Solid and dashed lines are the best fits to the bulge and disk sources, respectively.

bulge sources and $I(v = 2) = 1.07[\dot{M}/1 \times 10^{-6}(M_\odot\ \mathrm{yr}^{-1})]^{0.225}$ Jy km s^{-1} for the disk sources. It seems to indicate that the integrated SiO maser intensity increases weakly with mass-loss rate for both bulge and disk sources, and that there is no statistically significant difference between the bulge and disk sources.

The large scatter of the data points from the best fit in Figure 6 is due to the strong time variation of SiO maser intensity. We have observed SiO masers several times for the last 2 yr (but not periodically) and found that the intensity of a particular

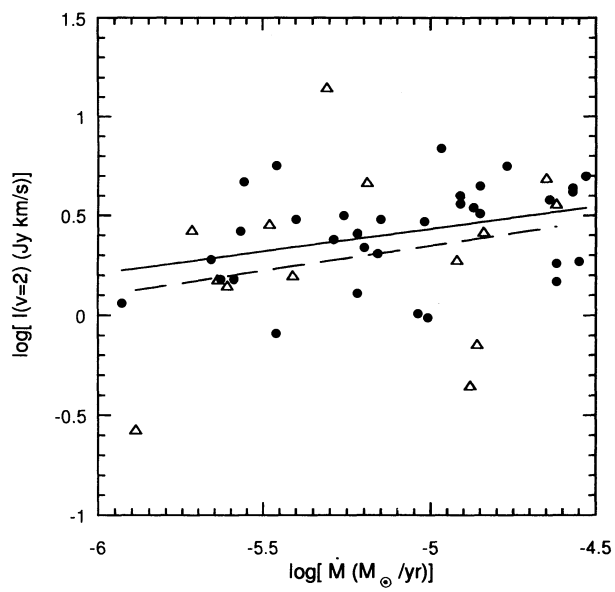

FIG. 6.—Mass-loss rate vs. maser integrated intensity (corrected for the distance). The filled circles are for the bulge source, and the triangles, for the disk sources. The solid and dashed lines are the best fits to the bulge and disk sources, respectively.

TABLE 4

SiO Maser Sources with Known Distances

IRAS Name	V_s (km s^{-1})	V_{rot} (km s^{-1})	log [$I(v = 1)$][a]	log [$I(v = 2)$][a]	R (kpc)
16508−3120.....	−127.6	243.1	0.41	0.70	2.40
16537−3112.....	−145.0	177.3	0.30	0.41	1.45
17002−2830.....	−154.1	171.0	−0.09	0.11	0.81
17005−2946.....	38.1	−145.0	0.63	0.67	3.34
17030−2801.....	−64.8	79.3	0.57	0.64	0.76
17042−2833.....	3.8	−21.7	−0.56	0.56	3.82
17046−2758.....	−108.3	507.3	0.24	0.42	2.72
17062−2758.....	−36.9	277.2	−0.02	−0.14	4.14
17172−2435.....	−73.6	−2921.5	0.45	0.43	3.22
17202−2244.....	−28.8	−320.9	−0.47	−0.57	4.13
17229−2059.....	31.8	36.0	0.80	0.84	0.73
17241−2202.....	−45.9	−109.1	0.29	0.54	1.27
17244−2131.....	−103.4	−171.5	0.24	0.31	1.00
17264−2037.....	21.8	41.4	0.79	0.56	1.44
17267−2122.....	−7.0	−23.8	0.55	0.62	2.27
17287−1955.....	41.8	55.4	0.40	0.27	1.18
17292−1931.....	100.4	109.1	0.42	0.38	1.04
17304−1933.....	123.7	647.0	0.45	0.69	5.07
17323−1833.....	11.9	12.5	0.63	0.18	1.20
17357−1704.....	−38.7	−38.8	0.03	−0.01	1.39
17365−1641.....	−20.6	−27.7	0.29	0.18	1.95
17367−1656.....	13.6	21.2	0.71	0.65	2.22
17382−1704.....	−6.5	−23.4	−0.35	−0.35	5.13
17440−1404.....	262.8	293.5	0.45	0.48	2.14
17457−1301.....	49.7	86.4	0.19	0.28	3.62
17457−1347.....	−0.3	−0.4	−0.18	0.18	2.54
17555−3847.....	−78.1	249.9	0.49	0.46	3.41
17599−3746.....	−17.6	19.5	0.20	0.01	0.96
18024−3543.....	−114.2	1415.3	1.21	1.15	6.97
18060−3451.....	−7.0	83.7	0.10	0.15	4.71
18163−3106.....	0.6	3.9	−0.17	−0.09	1.84
18217−2906.....	113.8	243.3	0.82	0.75	1.31
18220−2920.....	165.8	166.6	0.31	0.28	0.58
18224−2756.....	5.9	10.4	0.52	0.42	1.37
18240−2832.....	161.1	407.4	0.55	0.50	1.82
18260−2619.....	46.4	49.5	0.56	0.60	1.12
18264−2720.....	106.7	116.9	0.26	0.26	1.01
18267−2603.....	122.2	122.2	0.26	0.17	1.09
18274−2657.....	94.4	119.8	0.69	0.67	1.25
18279−2707.....	−17.5	−17.5	0.32	0.34	0.97
18282−2536.....	146.3	179.3	0.42	0.51	1.44
18287−2611.....	52.3	55.4	0.39	0.58	1.17
18290−2459.....	93.8	504.2	0.13	0.20	6.84
18290−2642.....	101.3	127.8	0.56	0.47	1.32
18307−2604.....	−35.7	−42.6	0.10	0.06	1.38
18341−2357.....	−22.4	−24.8	0.52	0.48	1.64
18347−2351.....	−11.6	−14.1	0.65	0.75	1.84

[a] log [$I(v = 1$ and $2)$] is logarithm of the integrated intensity (Jy km s^{-1}) when the star is placed at a distance of 8.6 kpc (corrected for the distance).

SiO maser can vary at least by a factor of 10. Nakada et al. (1993) discussed the relation between the time variation and the frequency distribution of the SiO maser flux. The detection of SiO masers may be possible only at the intensity maximum for the bulge sources. On the other hand, for relatively close disk sources, we may detect SiO even if it is weak. Furthermore, the mass-loss rates estimated by Whitelock et al. (1991) (from an expression given by Pottasch 1984 with assumed radii and expansion velocities) may contain uncertainty for the bulge *IRAS* sources. Figure 6 may not show a clear dependence of integrated intensity on the mass-loss rate due to these uncertainties. The properties of the dust grains and shell parameters of bulge sources among our sample may be different. However, the distribution of infrared colors, $C[25/12]$, of our sample are relatively homogeneous and the uncertainty factor for the estimation of the mass-loss rate must be minimized.

3.3. *Rotation of the Bulge*

The rotation of the Galactic bulge has been investigated using planetary nebulae (Kinman, Feast, & Lasker 1988), Mira variables (Menzies 1990), and K giants (Minniti et al. 1992). Nakada et al. (1993) obtained a rotation velocity of the bulge of about 9.9 km s^{-1} deg^{-1} based on 15 SiO maser sources detected in the Galactic bulge. In this paper, we have also obtained the rotation velocity of the bulge. We assume that the radial velocities of the SiO masers coincide with the stellar

velocity within an accuracy of a few km s^{-1} (see Jewell et al. 1991).

In this paper, we will take advantage of the fact that many of the sources in the 7°–8° strips have known distances. We will discuss the average rotation of the bulge for the sources within 2.5 kpc from the Galactic center. The previous study (Nakada et al. 1993) included all the SiO maser stars in the bulge direction. The contamination of the sample with disk sources was not considered. In this study, we exclude the disk sources.

We have plotted the l-V_s diagrams (Fig. 7) for the north ($b > 0$; *circle with dot*) and south ($b < 0$; *crosses*) sources separately. The best fit for the 33 sources within a distance of 2.5 kpc from the Galactic center is $V_s = -24.7(\pm 18.4) + 10.4$ (± 2.6) (l deg^{-1}) km s^{-1}. This rotation curve represents the average rotation of the SiO maser stars in the Galactic bulge system. Stars are assumed to be uniformly rotating around the Galactic center (with a constant angular velocity with radius). Deviations from the uniform circular orbits can account for the scatter in Figure 7. However, we noticed two problems with this simple fitting procedure: (1) The crossing point at $l = 0°$ does not coincide with $V_s = 0$, which may be due to the motion of the local standard of rest toward the Galactic center, or to other observational selection effects (see Izumiura et al. 1993); and (2) the north sources are shifted systematically toward the lower velocity side (see Fig. 7). It seems that the slope, i.e., the rotational rate, is less for the southern strip sources than that for the northern strip sources. The present sample contains only one southern negative longitude source, however. So we believe that the difference of the rotation rate between the northern and southern strips is not significant. These two problems are common in the analysis of larger samples of the bulge SiO masers with various Galactic latitudes. A full presentation of the analysis of these remarkable aspects of the rotation curve of the Galactic bulge will be a subject of the future papers. Here we will discuss only the velocity shift of north and south sources.

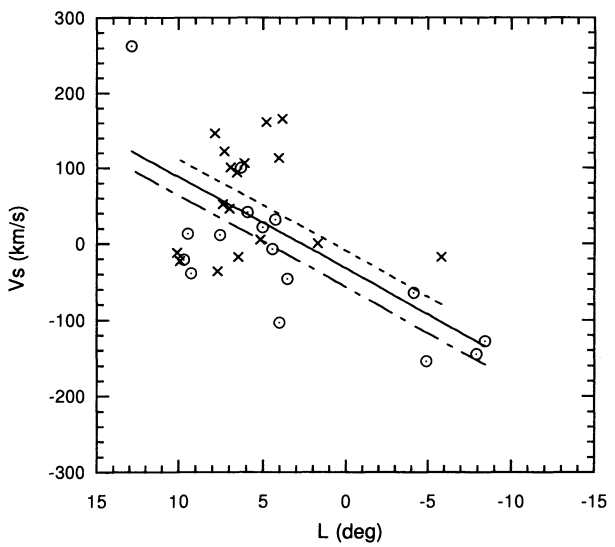

FIG. 7.—The radial velocity in Galactic standard of rest, V_s, versus Galactic longitude, l. The open circles indicate the northern ($7° < b < 8°$) sources and the crosses mark the southern ($-8° < b < -7°$) sources. The solid line is the least-squares fit for all the bulge sources (within 2.5 kpc). The dot-dashed line is the least-squares fit to the northern sources and the broken line to the southern sources, using the same slope of all the bulge sources.

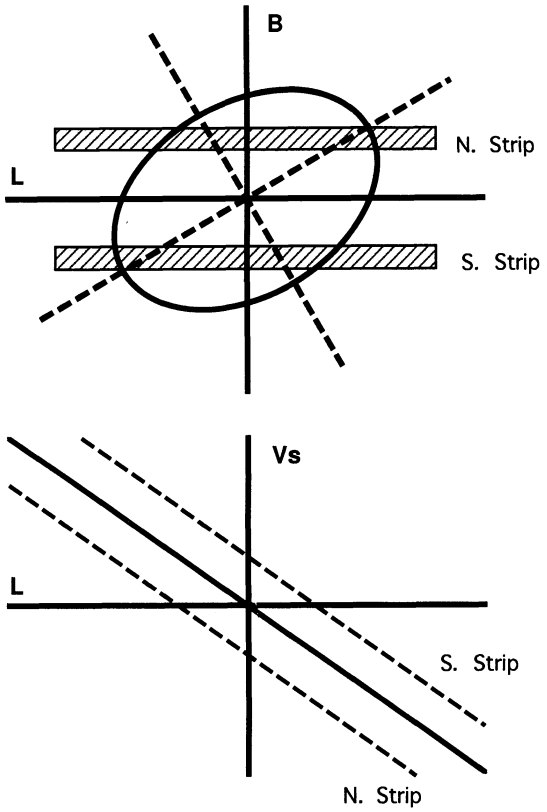

FIG. 8.—A tilt of the bulge with respect to the Galactic equator (*upper panel*) causes the shift of the rotation curve on the northern and southern strips (*broken lines* in the lower panel) if plotted against the Galactic latitude.

One of the interpretations for this shift of the rotation curve between the northern and southern strips is that it is due to a tilt of the bulge rotation axis to the Galactic longitude circle ($l = 0°$). When the bulge rotation axis is tilted as shown in the upper panel of Figure 8, the zero rotation velocity occurs at negative longitude for the north strip sources and at positive longitude for the south strip sources. As a result, the rotation curve in the diagram splits into two as shown in the lower panel of Figure 8. Using the slope fitted to the entire sample, we obtained $V_s = -51.1(\pm 17.0) + 10.4(l$ deg$^{-1})$ km s^{-1} and $V_s = 0.2(\pm 19.0) + 10.4(l$ deg$^{-1})$ km s^{-1} for the northern and southern strips, respectively. The mean velocity at the zero latitude is -25.4 km s^{-1}.

From the velocity difference between northern and southern rotation curves and the average rotation rate (51.2 km s^{-1} and 10.4 km s^{-1}, respectively), the shift in longitude at zero velocity of each strip is derived as $2°.5(^{+3°.0}_{-2°.0})$. From this value, we obtain a tilt angle of the bulge axis as $18°(^{+18°}_{-14°})$ with respect to the Galactic longitude circle ($l = 0°$).

The tilt angle of the bulge which we derived in the present paper coincides well with the tilt angle of 22° derived for the nuclear gas disk from an analysis of the H I distribution at $|l| < 12°$ (Burton & Liszt 1978). A revised model of the ^{12}CO nuclear disk by Burton & Liszt (1992) (at $|l| < 10°$ near the Galactic center) gave a maximum warp angle of 13° with a line of node rotated 45° from the Sun–Galactic center line. Heiligman (1987) reported a tilt of 5° of the nuclear disk from the ^{13}CO observations within $|l| < 2°$ and $|b| < 0°.5$. Blitz & Spergel (1991b) found a tilt angle of 3°–6° based on the analysis of the brightness distribution of the 2.4 μm bulge emission. The

sense of the tilt obtained by these papers coincides with the present result.

Several other explanations are possible for the velocity shift of the northern and southern sources in Figure 7. For instance, an extreme model is that the bulge is rotating not uniformly but differentially with the latitude. In fact, it can be seen from Figure 7 that the rotation rate of the southern strip is smaller from the rate of the northern strip (note that this depends strongly on the one source point with the negative longitude). The other alternative is the streaming motion of stars in the bulge with different streaming velocities between southern and northern sources. It may be deduced from Figure 7 that, on average, southern stars are approaching us and northern stars are receding from us at the positive longitude. It is not clear whether the stars with a negative longitude have the same or opposite tendency (because of the small number of the data points). However, any dynamical models of the bulge stellar system (see the review by de Zeeuw 1993) did not predict such a north-south asymmetry of stellar motion. Therefore these alternative explanations do not have a strong physical basis. We believe that the tilt of rotation axis is the best interpretation of the present result at least at present.

Keeping the problems of analyzing the rotation curve in mind, we have analyzed the data of 33 bulge sources which are located within 2.5 kpc from the Galactic center. The small tilt angle of the rotation axis of the bulge will be neglected in the later analysis. From the radial velocity in the Galactic standard of rest (Kerr & Lynden-Bell 1986), we can calculate the rotation velocity of a source V_{rot}, by assuming that the observed velocity is a projection of the circular rotation velocities around the Galactic center to the line of sight (listed in Table 4). Figure 9 shows that the rotation velocity, V_{rot}, as a function of the distance from the Galactic center. The best linear fit is $V_{rot} = 50.8(\pm 14.2)$ km s^{-1}(R kpc^{-1}), and the standard deviation is 118 km s^{-1}. Here the axis of the bulge rotation is taken to be perpendicular to the line of sight. If it is inclined, a correction for the inclination has to be applied. The regression coefficient is 0.11, indicating that the rotation of the bulge does not appear very clearly in Figure 9. This is probably

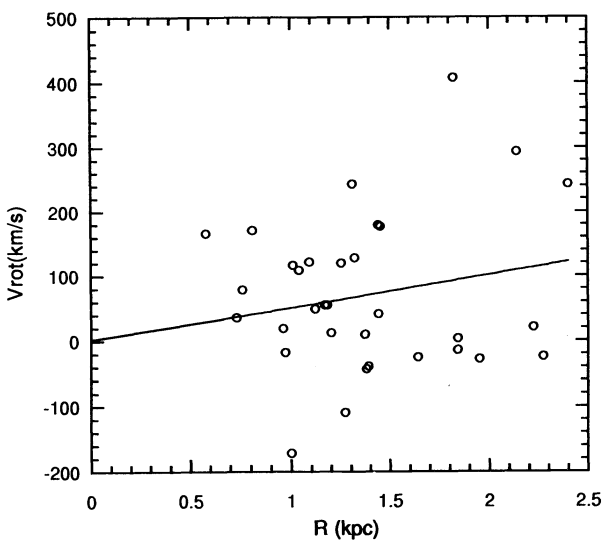

FIG. 9.—Circular rotation velocity of the SiO maser sources as a function of distance from the Galactic center. The solid line represents the best linear fit to the data.

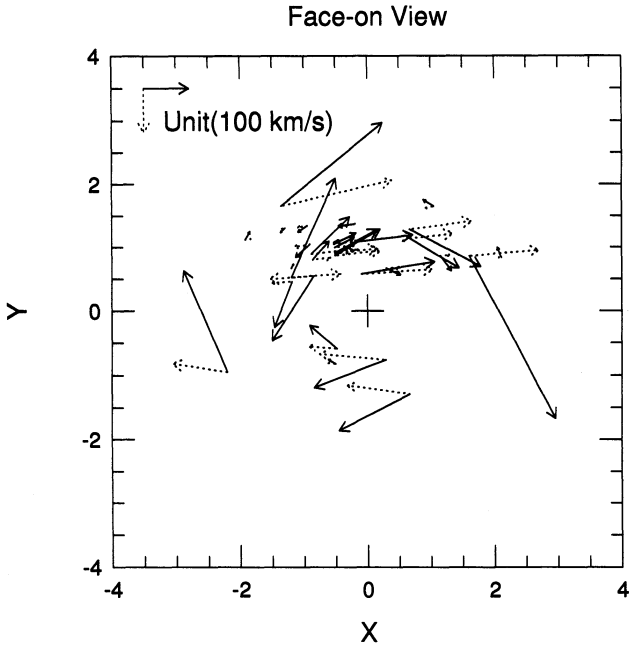

FIG. 10.—Top view of the Galaxy. The dotted arrows indicate the radial velocity (in the Galactic standard of rest), and the solid arrows indicate the rotational velocity calculated from the radial velocity assuming that the radial velocity is the projection of the rotation velocity along the line of sight. The origin of the arrow show the location of the SiO maser sources. The Galactic center is at (0, 0), and the Sun at (−8.6, 0).

because the estimation of the distance may contain probably about 20% errors and the radius from the Galactic center is not evaluated accurately. The rotation velocity derived from the V-l diagram (Fig. 7) is $V_{rot} = 71.4$ km s^{-1}(R kpc^{-1}). This value is rather independent of the errors in the distance estimation (but assuming the uniform rotation with a constant angular velocity). The rotation speed, 71.4 km s^{-1} kpc^{-1}, corresponds to an angular rotation rate of 7.3×10^{-8} rad yr^{-1}, or a rotation period of 8.6×10^{7} yr. This average rotation speed is considerably smaller than the rotational velocity of the nuclear gas disk (about 180 km s^{-1} at 0.5 kpc; Burton & Liszt 1978). It seems that the bulge stellar system is not corotating with the nuclear gas disk.

With the adopted distances, we have plotted a Galactic top view of the 33 bulge SiO maser sources in Figure 10. The Sun is located on the X-axis at (−8.6, 0). The Galactic center is at (0, 0), looking down on the Galactic bulge from the north Galactic pole. The origin of each dotted arrow is the position of the source and the length of the arrow is proportional to the radial velocity, V_s (in the Galactic standard of rest). The solid arrow shows the Galactic rotation velocity of each source.

3.4. *Individual Objects*

We have observed a number of *IRAS* objects in the Galactic bulge direction, and some of these sources were observed by others at different wavelengths. Some of these sources are bright at infrared wavelengths and may be foreground sources. We summarized the observations of these sources here.

3.4.1. *IRAS 17030−2801*

The 1612 MHz OH double peaks were detected at $V_{lsr} = -66.7$ and -31.1 km s^{-1} by te Lintel Hekkert et al. (1990) and Le Squeren et al. (1992). The center velocity (stellar velocity),

48.9 km s^{-1}, coincides well with the SiO emission peak velocities at $V_{lsr} = -49.1$ and -49.6 km s^{-1}. The expansion velocity of the circumstellar envelope is 17.7 km s^{-1} derived from the separation of OH 1612 MHz double peaks. This source was cataloged in the Atlas of *IRAS* Low-Resolution Spectra (LRS; Olnon et al. 1986) as a LRS class 14, exhibiting a very flat, featureless spectrum. The distance modulus indicates that this is a bulge source.

3.4.2. *IRAS 17070−2711 = KK Oph*

The position of this object coincides well with the position of KK Oph, a Herbig Ae/Be star (Weintraub 1990; see extensive spectral line studies in De Winter & The 1990). Water masers at 22 GHz were searched but not detected (Palla & Prusti 1993). Our detection of the SiO maser at $V_{lsr} = 22.9$ km s^{-1} (3.3 σ for the $v = 2$ transition) casts a doubt slightly on the identification of the *IRAS* source to Herbig Ae/Be star. However, the heliocentric velocity of the star, 10 km s^{-1}, ($V_{lsr} = 20.8$ km s^{-1}) and the Hα line width, 73 km s^{-1} (Finkenzeller & Jakovics 1984), are quite consistent with the SiO radial velocity, $V_{lsr} = 22.9$ km s^{-1}. Further confirmations of SiO for this weak source may be necessary.

3.4.3. *IRAS 17213−2219 = IRC 20359*

This source is one of the bright infrared sources in the direction of the bulge and probably a foreground source. No SiO maser was detected. Near-infrared photometry (Lockwood 1985) showed that this source is a M giant of a spectral type M7.8 and V magnitude is 13.1. The LRS class is 23, indicating a typical silicate feature (Olnon et al. 1986). Fouque et al. (1992) performed the *JHKLM* photometry of this source. Whitelock et al. (1991) found rather long period (722^d) for this source.

3.4.4. *IRAS 17382−1704*

The 1612 MHz OH double peaks were detected at $V_{lsr} = -53.3$ and -33.5 km s^{-1} by Le Squeren et al. (1992). The center velocity, -43.4 km s^{-1} coincides with the SiO peak velocity at $V_{lsr} = -43.9$ km s^{-1}. The expansion velocity of the envelope is 9.9 km s^{-1}. The LRS class is 27, indicating silicate emission. Near-infrared photometry (Whitelock et al. 1991; Fouque et al. 1992) indicates a period of 477^d. This is probably a foreground source.

3.4.5. *IRAS 18115−3237 = PK 359−07?*

This source is cataloged as PK 359−07.1, or M2-32, a well-observed planetary nebula in the Galactic bulge (e.g., Volk & Cohen 1990). Optical spectra of this planetary nebula have been taken by Acker et al. (1991). Volk & Cohen (1990) classified the *IRAS* LRS spectrum as F (flat unusual spectra), but it seems to exhibit a weak band at 17 μm. The radial velocity of PK 359−07 is $V_{lsr} = -40.1$ km s^{-1} (Schneider et al. 1983), which is not consistent with the observed SiO radial velocity, 22 km s^{-1}. The SiO feature is very wide (10 km s^{-1}) and the detection is confident. No 1612 MHz OH emission was detected (te Lintel Hekkert et al. 1990). Also, Whitelock et al. (1991) mentioned the presence of a confused near-infrared source in their Table 1. Considering these facts, we conclude that the SiO source is not associated with the planetary nebula PK 359−07.

3.4.6. *IRAS 18146−3110*

Van der Veen & Habing (1990) measured a period of 1600^d for this object and a luminosity of 7800 $L_\odot$. This period is not consistent with 525^d determined by Whitelock et al. (1992). This discrepancy is probably due to the small number of observed points in the former study. No SiO emission was detected in this object.

3.4.7. *IRAS 18290−2459 = V1902 Sgr*

This source is identified optically as a Mira variable, V1902 Sgr, with $m_v = 13.7$ mag and a period of 248^d.5. The period of the Mira variable does not agree with that obtained by Whitelock et al. (1991; 452^d). Its *IRAS* LRS class is 29, exhibiting strong silicate band emission (Olnon et al. 1986). We detected weak broad SiO emission at $V_{lsr} = 61.5$ km s^{-1} (Fig. 2*q*). This is probably a foreground source in the bulge direction. The distance modulus 11.3 is also consistent with this interpretation. The OH 1612 MHz double peaks were detected by te Lintel Hekkert et al. (1990; $V_{lsr} = 53.1$ and 68.4 km s^{-1}).

The other interesting objects are IRAS 18341−2357 and IRAS 18347−2351. These two objects lie in the close vicinity of the Galactic globular cluster, NGC 6652 (10′ and 21′ away from the center, respectively; Lynch & Rossano 1990). The distance of NGC 6652 from the Sun is about 3.1 kpc, and its angular diameter is 26′.2 (Lynch & Rossano 1990). According to Whitelock et al. (1991), the distances of these two *IRAS* sources are 7.8 and 9.4 kpc, respectively. Because of this difference in the distance, the globular cluster is a foreground object.

4. CONCLUSIONS

We have presented the observational results of a survey of 91 *IRAS* sources in the strips between $-15° < l < 15°$ and $7° < |b| < 8°$ in the SiO $J = 1$–0 and 2 transitions. SiO masers have been clearly detected in 53 sources, and probably in two additional sources. Based on distances derived from the period-luminosity relation and the periods of near-infrared intensity variation measured by Whitelock et al. (1991), we have divided the detected sources into bulge and disk sources. We have discussed the various properties of the SiO masers in the bulge sources. Integrated intensities of the SiO masers are weakly dependent on the stellar mass-loss rate. No systematic difference of the SiO maser properties seems to be present between the bulge and disk sources. From the measured radial velocities, the angular rotation velocity or the bulge stellar system is derived as 7.3×10^{-8} rad yr^{-1}, corresponding to a period of rotation as 8.6×10^7 yr. The Galactic top view of the distribution of the SiO sources and these rotation vectors was made as well.

We thank the staff of Nobeyama Radio Observatory for helping long periods of observations. We also thank R. Catchpole, M. Feast, K. Sekiguchi, and P. Whitelock in South African Astronomical Observatory for cooperative works and W. van Driel in Kiso Observatory and L. B. F. M. Waters in SRON Laboratory for Space Research Groningen for reading the manuscripts. One of the authors (H. I.) express his hearty thanks to the Ministry of Education, Science, and Culture of Japan for the financial support by Grant-in-Aid for Encouragement of Young Scientists (No. 047401270).

REFERENCES

Acker, A., Koppen, J., Stenholm, B., & Raytchev, B. 1991, A&AS, 89, 237
Blitz, L., & Spergel, D. N. 1991a, ApJ, 370, 205
———. 1991b, ApJ, 379, 631
Bujarrabal, V. 1994, A&A, in press
Burton, W. B., & Liszt, H. S. 1978, ApJ, 225, 842
———. 1992, A&AS, 95, 9
Cho, S., Kaifu, N., & Ukita, N. 1993, A&A, submitted
Deguchi, S., Nakada, Y., & Sahai, R. 1990, A&A, 230, 339
De Winter, D., & The, P. S. 1990, A&AS, 166, 99
de Zeeuw, T. 1993, in IAU Symp. 153, Galactic Bulges, ed. H. Dejonghe & H. J. Habing (Dordrecht: Kluwer), 191
Feast, M. W. 1987, in The Galaxy, ed. G. Gilmore & B. Carswell (Dordrecht: Reidel), 1
Finkenzeller, U., & Jakovics, I. 1984, A&AS, 57, 285
Fouque, P., Le Bertre, T., Epchtein, N., Guglielmo, F., & Kerschbaum, F. 1992, A&AS, 93, 151
Frogel, J. A. 1988, ARA&A, 26, 51
Gilmore, G. 1989, in The Milky Way as a Galaxy, ed. R. Buser & I. King (Geneva: Geneva Observatory), 281
Habing, H. J. 1987, in The Galaxy, ed. G. Gilmore & P. Carswell (Dordrecht: Reidel), 173
Habing, H. J., Olnon, F. M., Chester, T., Gillet, F., Rowan-Robinson, M., & Neugebauer, G. 1985, A&A, 152, L1
Heiligman, G. M. 1987, ApJ, 314, 747
Izumiura, H., et al. 1993, in IAU Symp. 153, Galactic Bulges, ed. H. Dejonghe & H. J. Habing (Dordrecht: Kluwer), 303
Jewell, P. R., Snyder, L. E., Walmsley, C. M., Wilson, T. L., & Gensheimer, P. D. 1991, A&A, 242, 211
Kent, S. M., Dame, T. M., & Fazio, G. 1991, ApJ, 378, 131
Kent, S. M., Mink, D., Fazio, D., Koch, D., Melnick, G., Tardiff, A., & Maxson, C. 1992, ApJ, 387, 181
Kerr, F. J., & Lynden-Bell, D. 1986, MNRAS, 221, 1023
Kinman, T. D., Feast, M. W., & Lasker, B. M. 1988, AJ, 95, 804
Le Squeren, A. M., Sivagnam, P., Dennefeld, M., & David, P. 1992, A&A, 254, 133
Lockwood, G. W. 1985, ApJS, 58, 167
Lynch, D. K., & Rossano, G. S. 1990, AJ, 100, 719
Manabe, S., & Miyamoto, M. 1975, PASJ, 27, 35
Menzies, J. W. 1990, in Bulges of Galaxies (ESO-CTIO Workshop), ed. B. J. Jarvis & D. M. Terndrup (Garching: ESO), 115
Minniti, D., White, S. D. N., Olzszewski, E. W., & Hill, J. M. 1992, ApJ, 393, L47
Nakada, Y., Deguchi, S., Hashimoto, O., Izumiura, H., Onaka, T., Sekiguchi, K., & Yamamura, I. 1991, Nature, 353, 140
Nakada, Y., Onaka, T., Yamamura, I., Deguchi, S., Ukita, N., & Izumiura, H. 1993, PASJ, 45, 179
Olnon, F. M., & IRAS Science Team, 1986, A&AS, 65, 607 (LRS)
Palla, F., & Prusti, T. 1993, A&A, 272, 249
Pottasch, S. R. 1984, in Planetary Nebulae (Dordrecht: Reidel), 201
Reid, M. J., Schneps, M. H., Moran, J. M., Gwinn, C. R., Genzel, R., Downes, D., & Rönnäng, B. 1988, ApJ, 330, 809
Rowan-Robinson, M., & Chester, T. 1987, ApJ, 313, 413
Schneider, S. E., Terzian, Y., Purgathofer, A., & Perinotto, M. 1983, ApJS, 52, 399
te Lintel Hekkert, P., Caswell, J. L., Habing, H. J., Haynes, R. F., & Norris, R. P. 1990, A&AS, 90, 327
Van der Veen, W. E. C. J., & Habing, H. J. 1990, A&A, 231, 404
Volk, K., & Cohen, M. 1990, AJ, 100, 485
Weinberg, M. D. 1992, ApJ, 384, 81
Weintraub, D. A. 1990, ApJS, 74, 575
Wood, P. R., Whiteoak, J. B., Hughes, S. M. G., Bessell, M. S., Gardner, F. F., & Hyland, A. R. 1992, ApJ, 397, 552
Whitelock, P., Feast, M., & Catchpole, R. 1986, MNRAS, 222, 1
———. 1991, MNRAS, 248, 276
Whitelock, P., Menzies, J., Feast, M., Marang, F., Carter, B., Roberts, G., Catchpole, R., & Chapman, J. 1994, MNRAS, 267, 711